



Design and synthesis of selective, dual fatty acid binding protein 4 and 5 inhibitors



Holger Kühne^{a,*}, Ulrike Obst-Sander^a, Bernd Kuhn^a, Aurelia Conte^a, Simona M. Ceccarelli^a, Werner Neidhart^a, Markus G. Rudolph^a, Giorgio Ottaviani^a, Rodolfo Gasser^a, Sung-Sau So^b, Shirley Li^b, Xiaolei Zhang^b, Lin Gao^b, Michael Myers^b

^aRoche Pharmaceutical Research and Early Development, Roche Innovation Center Basel, F. Hoffmann-La Roche Ltd, 4070 Basel, Switzerland

^bHoffmann-La Roche Inc., 340 Kingsland Street, Nutley, NJ 07110, USA

ARTICLE INFO

Article history:

Received 18 July 2016

Revised 18 August 2016

Accepted 20 August 2016

Available online 22 August 2016

Keywords:

FABP4

FABP5

Structure-based design

Quinoline derivatives

ABSTRACT

Dual inhibition of fatty acid binding proteins 4 and 5 (FABP4 and FABP5) is expected to provide beneficial effects on a number of metabolic parameters such as insulin sensitivity and blood glucose levels and should protect against atherosclerosis. Starting from a FABP4 selective focused screening hit, biostructure information was used to modulate the selectivity profile in the desired way and to design potent dual FABP4/5 inhibitors with good selectivity against FABP3. With very good pharmacokinetic properties and no major safety alerts, compound **12** was identified as a suitable tool compound for further in vivo investigations.

© 2016 Published by Elsevier Ltd.

Fatty acid binding proteins 4 and 5 (FABP4 and FABP5) are members of a family of small, soluble proteins which contribute to the trafficking of fatty acids within the cytosolic compartments of cells. The proteins have no catalytic function but transport hydrophobic fatty acids within the aqueous environment of the cytosol to the various destinations enabling fatty acid oxidation, membrane homeostasis or nuclear signaling. In addition, they are likely involved in signaling processes which are so far poorly understood.^{1–4}

FABP4 is highly expressed in adipose tissue, macrophages and endothelial cells. FABP5 is also expressed in macrophages and endothelial cells, as well as in skin and several other tissues.^{3,5}

We became interested in FABP4 and FABP5 as targets for inhibition after the discovery that genetic deletion of FABP4 and FABP5 in mice improves insulin sensitivity, lowers glucose, and protects against atherosclerosis.⁴ In a clamp study in *ob/ob* mice, a specific FABP4 inhibitor (BMS309403) showed a reduction of hepatic glucose production, increased glucose uptake in muscle and adipose tissue, and reduction in hepatic steatosis, but no change in body weight and energy consumption. Additionally, this compound showed a decrease in atherosclerotic plaque formation in ApoE KO mice.⁶

* Corresponding author. Tel.: +41 616889176.

E-mail address: holger.kuehne@roche.com (H. Kühne).

In humans, plasma levels of FABP4 are increased in patients with metabolic syndrome and atherosclerosis.⁷ In addition, there is growing evidence for involvement of FABP4 in angiogenesis⁸ and growth of certain tumors.⁹ Increased levels of FABP5 have been found in human breast cancers and experimental results suggested that FABP5 is critical for mammary tumor development.¹⁰

The FABP family comprises nine isoforms, which differ in their sequence and tissue distribution, but have remarkably similar structures.⁴ Our goal was to provide a dual FABP4/5 inhibitor selective against other FABP isoforms with good physicochemical and pharmacokinetic properties suitable as a tool for testing in models of metabolic diseases, angiogenesis or tumor growth. As selectivity filter, we chose activity against the structurally closely related FABP3 and the less similar FABP1.

A number of FABP inhibitors have been described in the literature. The pyrazole BMS309403 (**1**)^{6,11} has been used extensively as a tool for FABP4 inhibition, both in vitro and in vivo.^{12,13} Other structurally diverse compounds include indoles from Biovitrum (**2**),¹⁴ thiophenes from the University of Minnesota (**3**),¹⁵ as well as non-carboxylic acids from Biovitrum (**4**),¹⁶ and Merck (**5**).¹² We tested a selection of published FABP inhibitors in our FABP binding assays measuring the displacement of a fluorescently labeled fatty acid.¹⁷ However, we could not identify dual acting FABP4/5 inhibitors of reasonable selectivity against other FABP isoforms. Moreover, most compounds had no activity against FABP5 (Fig. 1).

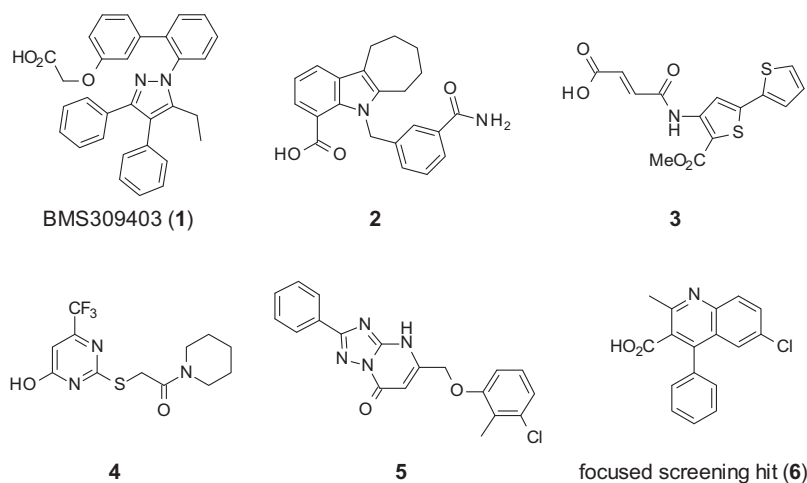


Figure 1. Structure of some published FABP4 inhibitors and focused screening hit quinoline **6**.

To identify novel chemical starting points for our program we conducted a focused screen against FABP4 and profiled the hits additionally against the FABP3 and 5 isoforms. The screening set consisted of about 1200 molecules from the Roche compound library which were selected based on 2D^{18,19} and 3D similarity²⁰ to published FABP inhibitors. Although a number of structurally diverse candidates were found, most of the compounds were devoid of FABP5 activity. We decided to select hits for optimization based on their physicochemical and eADME properties and tried to design-in the desired dual FABP4/5 activity and selectivity against other FABP isoforms, especially FABP3. The quinoline carboxylic acid **6** appeared to be a good starting point (Table 1).

Despite the fact that compound **6** did not have the desired dual FABP4/5 selectivity profile, it turned out to be a very attractive starting point due to its favorable eADME properties such as high solubility, good permeability, low clearance in both human and mouse microsomes and low potential for drug–drug interactions. Considering the mostly lipophilic nature of the FABP4 binding pocket, compound **6** has a surprisingly low $\log D$, which in combination with the low molecular weight offered good opportunities for further optimization. In addition, a crystal structure from the complex of **6** with FABP4 was obtained early in the program revealing its binding mode (Fig. 2). The ligand occupies a buried hydrophobic pocket with limited solvent access. The carboxylate group is engaged in a direct hydrogen bond with the guanidinium group of Arg127 as well as in two water-mediated hydrogen bonds with Tyr129. A large number of apolar π – π and dispersion interactions are made between the remainder of the inhibitor and the many lipophilic side chains pointing into the binding cavity.

One structure-based approach to modulate the selectivity profile of a small molecule is to exploit sequence differences in the

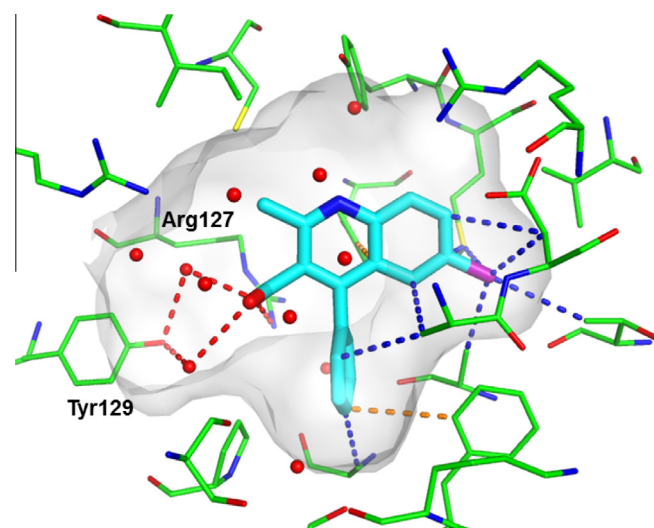


Figure 2. Crystal structure of human FABP4 with compound **6** (PDB code: 5edb). Protein residues are colored in green and the ligand in cyan. Water molecules are shown as red spheres. Favorable protein–ligand interactions²³ are shown as dashed lines (red: hydrogen bond, orange: π – π , blue: dispersion).

ligand binding site. To identify these regions, we overlaid the crystal structure from Figure 2 with co-crystal structures of all three isoforms with the common ligand palmitic acid. From this analysis, several amino acids could be identified that are in close proximity to bound compound **6** and differ between FABP4, 5 and 3. As illustrated in Figure 3, four potential selectivity regions S1–S4 were identified, suggesting small differences in pocket size and shape between the three isoforms. Regions S1, S3 and S4 were most attractive as they could be readily reached with different substituents from the 4-phenyl quinoline scaffold of **6**.

We first focused our attention on region S4 because our analysis suggested a smaller binding pocket for FABP3 due to the presence of three Leu side chains which are bulkier compared to the set of Ile, Val, Cys residues in FABP4 and 5. Moreover, the quinoline 2-position was ideally suited to target this region. Increasing the size of the quinoline 2-substituent from methyl to isopropyl (compound **7**) to provoke a steric clash with FABP3 already changed the activity profile in the desired way. Not only did this modification lead to a drop of the FABP3 inhibition constant from 0.093 to 0.39 μM , it also afforded the first compound in this series with measurable FABP5 activity. The concomitant strong gain in binding

Table 1
Properties of screening hit **6**

hFABP4: K_i (μM)	0.105
hFABP5: K_i (μM)	>23.2
hFABP3: K_i (μM)	0.093
$\log D$ (pH 7.4)	–0.44
Solubility ($\mu\text{g}/\text{ml}$) ^a	>355
Permeability (10^{-6} cm/s) ^b	0.23
CYP450 (3A4/2D6/2C9): IC_{50} (μM)	>50/>50/>50
CL_{int} h/m ($\mu\text{l}/\text{min}/\text{mg}$ of protein) ^c	<10/<10

^a LYSA²¹.

^b PAMPA²².

^c From incubation with human and mouse liver microsomes.

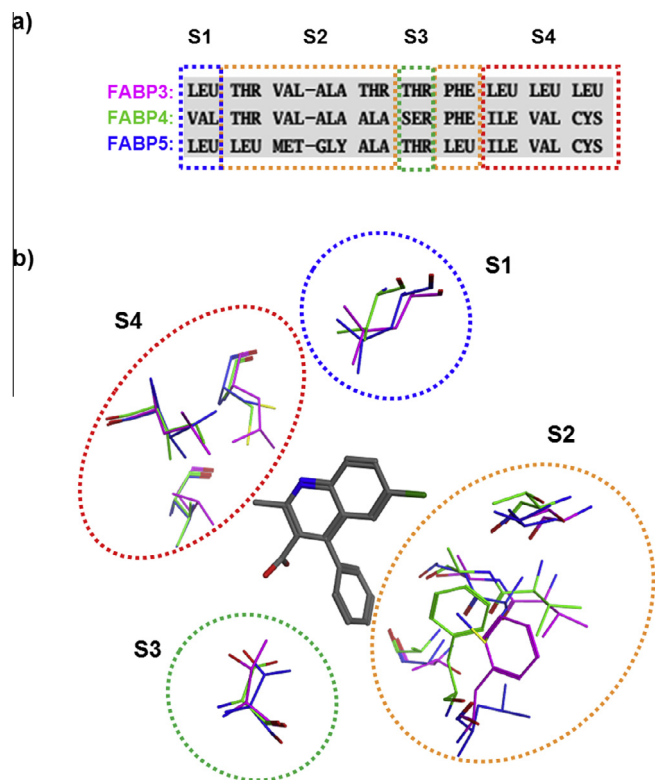


Figure 3. (a) 1-D sequence view of amino acid differences of human FABP3, 4, and 5 in close contact (≤ 5.5 Å) to bound compound **6** as identified from an overlay of the co-crystal structures: FABP4-compound **6** (PDB code: 5edb), FABP3-palmitic acid (2hmb), FABP4-palmitic acid (2hnx), and FABP5-palmitic acid (1b56). Selectivity regions are (hFABP4 numbering): S1 (V24), S2 (T30, V33, A34, A37, F58), S3 (S54), and S4 (I105, V116, C118). Numbering for hFABP3 is as for hFABP4; for hFABP5 numbers are shifted by +2. (b) 3-D structure view of (a). Only protein residues from the fatty acid-bound structures are shown.

to FABP4 suggests that the S4 pocket was not optimally filled with the original methyl substituent. Further increasing the size of the quinoline 2-substituent to piperidinyl led to compound **8**, which keeps its activity on FABP4 and 5, but has >20-fold reduced FABP3 affinity compared to **7**. An overlay of the complex crystal structure of **8** in FABP4 with **6** in FABP3 indicates strong repulsive interactions of the piperidinyl substituent in FABP3, which likely explains the >100-fold weaker FABP3 activity of **8** versus **6** (Fig. 4a).

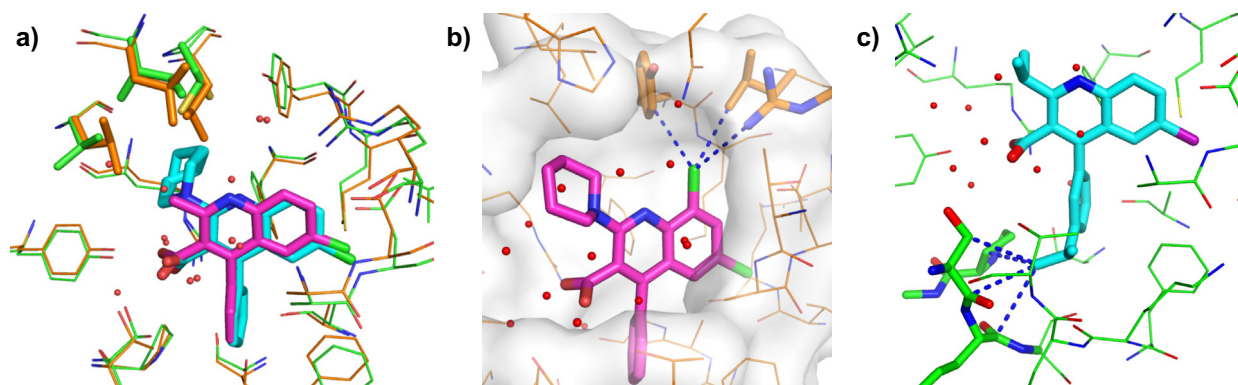


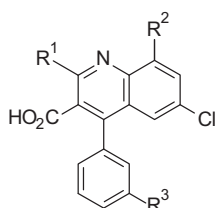
Figure 4. (a) Overlay of co-crystal structures of human FABP4 with compound **8** (protein: green, ligand: cyan, PDB code: 5edc) with human FABP3 bound to compound **6** (protein: orange, ligand: magenta, PDB code: 5hz9). Protein residues of selectivity region S4 are highlighted as sticks. Electron density is rather weak for the piperidinyl group in 5edc. Two conformations for the sidechain of Cys118 and for the ligand piperidinyl were used to model the electron density of this complex. (b) Crystal structure of human FABP3 with compound **9** (PDB code: 5hz8). Protein residues are colored in orange and those residues with short contacts < 4.0 Å (dashed blue lines) to the 8-chlorine substituent of the ligand (magenta) are highlighted as sticks. (c) Crystal structure of human FABP4 with compound **11** (PDB code: 5hz6). Protein residues are colored in green and those residues with short contacts < 4.0 Å (dashed blue lines) to the isopropyl substituent at R³ of the ligand (cyan) are highlighted as sticks.

Next we probed selectivity region S1 with small substituents in the quinoline 8-position. This region contains Leu in FABP3 and FABP5, and a smaller Val residue in FABP4. Replacing the hydrogen in 8-position of compound **8** by $-Cl$ (**9**) or $-Me$ (**10**) led to a ~ 5 -fold affinity increase in FABP5 and to a >25-fold gain for FABP3. K_i values for FABP4 changed only slightly within a factor of 2. Due to the strong affinity enhancement for FABP3, compounds **9** and **10** are no longer selective against this isoform. A subsequently determined crystal structure of **9** in complex with FABP3 could rationalize the improved binding to this isoform (Fig. 4b). The additional $-Cl$ substituent nicely fills a small cavity in the FABP3 binding site which is formed by the side chains of Tyr20, Leu24, and Arg79, and makes three short non-bonded contacts with distances < 4.0 Å to each of these amino acids. Further increasing the size of this substituent, e.g. by an ethyl substituent, led again to an affinity decrease for FABP3, and to a smaller extent also for FABP5 (data not shown).

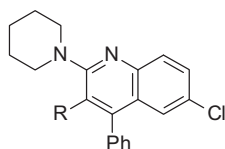
In line with the sequence conservation in this part of the binding site (S1), the SAR at the 8-position is qualitatively similar for FABP3 and FABP5. The much steeper SAR for FABP3 suggests that this isoform might be more rigid in selectivity region S1 compared to FABP5.

Finally, we explored selectivity region S3 by addition of meta-substituents to the quinoline 4-phenyl moiety. We discovered that this position is suitable to obtain very selective FABP4 ligands such as compound **11**. The binding mode of compound **11** in FABP4 (Fig. 4c) shows several favorable dispersion interactions of the isopropyl-substituent at R³ with carbon atoms of the protein. The crystal structure suggests that only the smaller Ser54 residue in FABP4 is able to accommodate an isopropyl group at this position while the bulkier Thr present in FABP3 and FABP5 might cause a steric clash with the ligand resulting in FABP4 selective compounds (Table 2).

For the most selective dual FABP4/5 inhibitor **8**, bioisosteric replacements of the carboxylic acid group were investigated (Table 3). Tetrazole (**12**), oxadiazolone (**13**), and oxadiazolthione (**14**) derivatives all retain good binding affinities to FABP4. With all replacements the affinity to FABP5 could be improved and selectivity against FABP3 was maintained. Despite a favorable selectivity profile, the oxadiazole derivatives **13** and **14** were less attractive, as these carboxylic acid replacements render the compounds considerably more lipophilic and less soluble. A crystal structure of **12** in FABP5 was determined revealing interesting intermolecular interactions of the tetrazole head group (Fig. 5).

Table 2
Exploration of selectivity

R ¹					
R ² /R ³	H/H	H/H	Cl/H	CH ₃ /H	H/iPr
No.	7	8	9	10	11
hFABP4: K _i (μM)	0.012	0.022	0.016	0.013	0.016
hFABP5: K _i (μM)	1.2	0.50	0.12	0.10	4.3
hFABP3: K _i (μM)	0.39	10.2	0.40	0.10	22.4
logD (pH 7.4)	-0.11	0.82	1.67	2.14	1.67
Solubility (μg/ml)	>370	>435	395	>465	>455
Permeability (10 ⁻⁶ cm/s)	1.96	6.99	2.98	1.78	6.47
CYP450 (3A4/2D6/2C9): IC ₅₀ (μM)	>50/>50/>50	>50/>50/>50	>50/>50/21	16/42/12	>50/>50/9.7
CL _{int} h/m (μl/min/mg)	<10/<10	<10/<10	<10/<10	<10/<10	17/<10

Table 3
Carboxylic acid bioisosteres

R			
No.	12 (RO6806051)	13	14
hFABP4: K _i (μM)	0.011	0.020	0.007
hFABP5: K _i (μM)	0.086	0.167	0.133
hFABP3: K _i (μM)	2.3	9.7	4.1
logD (pH 7.4)	2.12	3.53	2.87
Solubility (μg/ml)	>420	<1	108
Permeability (10 ⁻⁶ cm/s)	3.4	0.06	1.44
CYP450 (3A4/2D6/2C9): IC ₅₀ (μM)	>50/33/13	>50/38/11	15/47/3.5
CL _{int} h/m (μl/min/mg)	<10/<10	19/40	<10/18

While all four nitrogen lone pairs of the tetrazole are engaged in either direct (Arg129, Tyr131) or water mediated hydrogen bonds, an additional dispersion interaction between the C_γ of Thr56 and the apolar side of the head group can be detected. We hypothesize that the additional gains in binding affinity for FABP5 and FABP3 for the carboxylate replacements might be due to this additional dispersion interaction which is not possible with the analogous Ser in FABP4.

As a potent dual FABP4/5 inhibitor with good selectivity and an appealing eADME profile, tetrazole derivative **12** (RO6806051) was profiled in more detail. When **12** was tested against a panel of 72 receptors, channels, transporters and 25 enzymes, it showed no significant interaction with any of the targets at a concentration of 10 μM. In addition, compound **12** exhibited no interaction with the hERG channel (IC₂₀ > 10 μM) and tested negative in the Ames and micronucleus test. In vivo pharmacokinetic studies in mouse revealed a very attractive profile with nearly complete oral

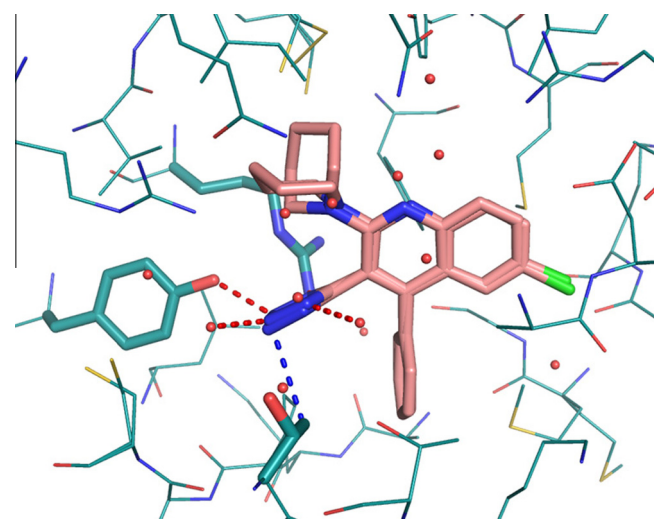


Figure 5. Crystal structure of human FABP5 with compound **12** (PDB code: 5hz5). Protein residues are colored in green and the ligand in salmon. Water molecules are shown as red spheres. Protein residues in contact with the tetrazole head group are highlighted as sticks. Electron density is weak for the piperidinyl group. Two conformations for the sidechain of Cys120 and for the ligand piperidinyl were required to model the electron density. Intermolecular interactions of the ligand tetrazole are shown as dashed lines (red: hydrogen bond, blue: dispersion).

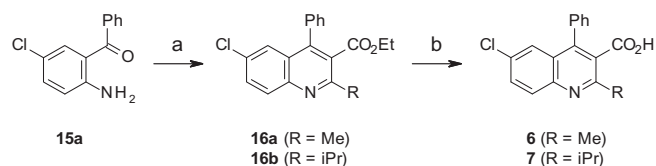
bioavailability, low clearance, moderate volume of distribution and a half-life of more than 5 h after oral application (Table 4).

Detailed synthetic pathways to new quinoline derivatives **7–14** are depicted in Schemes 1–5, respectively.¹⁷ Compounds **6** and **7** were obtained by condensation reaction of amino-benzophenone **15a** with the appropriate β-ketoester and subsequent ester cleavage (Scheme 1).

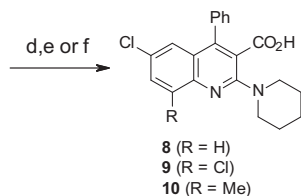
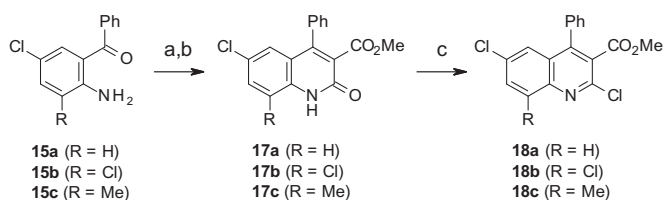
Synthesis of compounds **8**, **9** and **10** (Scheme 2) started with amide formation between amino-benzophenone derivatives **15a–c** and methyl 3-chloro-3-oxopropanoate followed by cyclization to quinolone derivatives **17a–c** with NaOMe. Treatment of **17a–c** with POCl₃ afforded 2-chloro-quinoline derivatives **18a–c**. Compound **8** was prepared from **18a** by reaction with piperidine and subsequent ester cleavage. Due to the strong steric hindrance of

Table 4
Pharmacokinetic properties of **12** in mouse

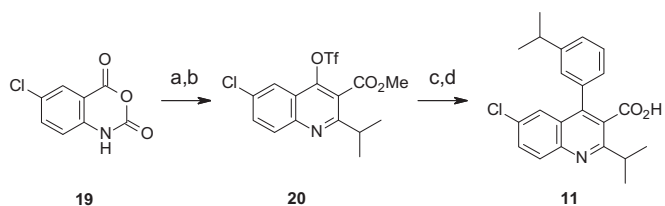
Parameter	Value
<i>iv</i> dose (3.3 mg/kg)	
CL (ml/min/kg)	5.8
V_{ss} (l/kg)	3.3
<i>po</i> dose (8.4 mg/kg)	
Bioavailability <i>F</i> (%)	99
$t_{1/2}$ (h)	5.8
PPB (% unbound)	<0.26



Scheme 1. Reagents and conditions: (a) for R = Me: ethyl 3-oxobutanoate, TMSCl, DMF, 100 °C (sealed tube), o.n., 60%; for R = iPr: ethyl 4-methyl-3-oxo-pentanoate, Yt(OTf)₃, EtOH, rt, o.n., 28%; (b) for R = Me: NaOH, EtOH, reflux, o.n. 56%; for R = iPr: KOH, MeOH/H₂O/THF, 65 °C, 50 h, 77%.



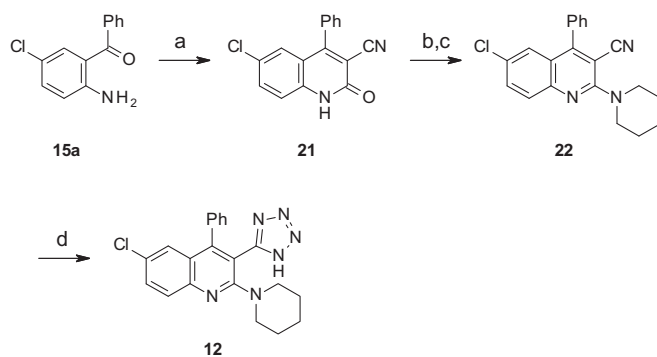
Scheme 2. Reagents and conditions: (a) methyl 3-chloro-3-oxopropanoate, DCM, 0 °C to rt, 3 h, 93–95%; (b) NaOMe, MeOH, rt, 1 h, 90–99%; (c) POCl₃, reflux, o.n., 84–92%; (d) for R = H: piperidine, TEA, DMF, 130 °C (microwave), 0.3 h, 74%; (e) Lil, pyridine, reflux, o.n., 99%; (f) for R = Cl, Me: piperidine, pyridine, reflux (sealed tube); 48 h, 50–99%.



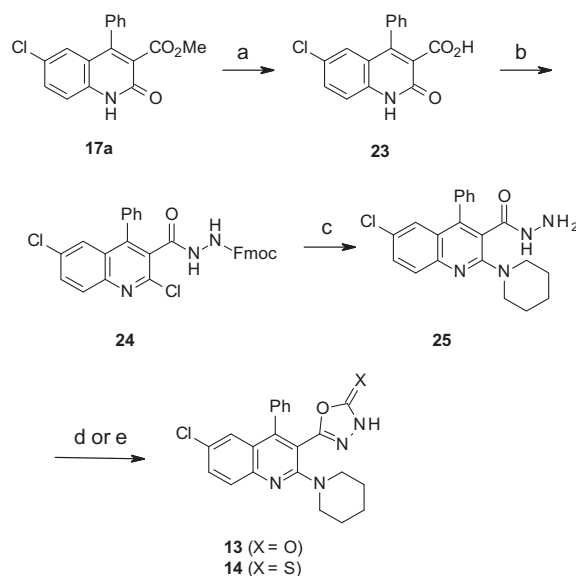
Scheme 3. Reagents and conditions: (a) methyl 4-methyl-3-oxo-pentanoate, NaH, DMA, 0–120 °C, 1 h, 42%; (b) NaH, PhN(Tf)₂, DMF, rt, 2 h, 95%.

the ester group, cleavage is most effective with Lil in pyridine. Compounds **9** and **10** were prepared from **18b** and **18c** in one step with piperidine in pyridine in a sealed tube, effecting the nucleophilic substitution reaction and the ester cleavage simultaneously.

Starting from isatoic anhydride derivative **19**, reaction with methyl 4-methyl-3-oxo-pentanoate followed by reaction with *N*-phenyl-bis(trifluoromethanesulfonylimide) provided triflate deriva-



Scheme 4. Reagents and conditions: (a) ethyl 2-cyanoacetate, CeCl₃·7H₂O (cat.), 200 °C (microwave), 0.5 h, 32%; (b) POCl₃, reflux, 1 h, 76%; (c) piperidine, TEA, DMF, 120 °C (microwave), 0.3 h, 85%; (d) azidotrimethyltin, xylene, 120 °C, 48 h, 49%.



Scheme 5. Reagents and conditions: (a) LiOH, EtOH, 50 °C, 72 h, 95%; (b) (i) POCl₃, 120 °C, o.n., (ii) Fmoc-hydrazine, DCM, rt, 4 h, 60%; (c) piperidine, TEA, DMF, 120 °C, 3 h, 82%; (d) CDI, TEA, THF, rt, 2 h, 87%; (e) CS₂, KOH, EtOH, reflux, o.n., 74%.

tive **20** which can be further elaborated into compound **11** by Suzuki coupling with (3-isopropylphenyl)boronic acid and subsequent ester cleavage (Scheme 3).

The synthesis of tetrazole derivative **12** started by condensation reaction of **15a** and ethyl 2-cyanoacetate to obtain quinolone **21**. Chlorination of **21** with POCl₃ followed by reaction with piperidine provided intermediate **22** which was converted into **12** by reaction with azidotrimethyltin (Scheme 4).

Oxadiazole derivatives **13** and **14** were synthesized starting from quinolone **17a** (Scheme 5). Reaction of **17a** with LiOH provided intermediate **23** which was reacted with POCl₃ to convert the carboxylic acid to the acid chloride and the quinolone into the corresponding 2-chloro-quinoline at the same time. The crude product of this chlorination reaction was immediately reacted with Fmoc protected hydrazine to obtain hydrazide derivative **24**. Treatment of **24** with piperidine introduced the piperidinyl substituent in the quinoline 2-position and simultaneously cleaved the Fmoc protecting group. Final reaction of **25** with CDI or CS₂ provided the oxadiazole derivatives **13** or **14** respectively.

In summary, we describe the structure-based design of a novel class of selective, dual FABP4/5 inhibitors. Several selectivity pockets could be identified by a structural bioinformatics analysis and

three of them were targeted with specific substitution on the quinoline core. This allowed us to change the selectivity profile from a dual FABP3/4 screening hit to a dual FABP4/5 inhibitor with optimized activity. The most advanced derivative **12** (RO6806051) has a very good selectivity profile, favorable physico-chemical properties and no major safety alert. The attractive pharmacokinetic profile in mouse makes **12** a suitable tool compound for further in vivo pharmacological investigations.

Acknowledgments

The authors gratefully acknowledge contributions by Eva Anna Krafft, Quentin Strebel, Marianne Rueher, Patrick Boissin, Noemi Raschetti, Jitka Weber, Andreas Ehler, Dave Solis and Jeff Tilley.

References and notes

- Hotamisligil, G. S.; Bernlohr, D. A. *Nat. Rev. Endocrinol.* **2015**, *11*, 592.
- Hardaway, A. L.; Podgorski, I. *Future Med. Chem.* **2013**, *5*, 1089.
- Furuhashi, M.; Ishimura, S.; Ota, H.; Miura, T. *Int. J. Inflammation* **2011**, 642612.
- Furuhashi, M.; Hotamisligil, G. S. *Nat. Rev. Drug Disc.* **2008**, *7*, 489.
- Thumser, A. E.; Moore, J. B.; Plant, N. J. *Curr. Opin. Clin. Nutr. Metab. Care* **2014**, *17*, 124.
- Furuhashi, M.; Tuncman, G.; Görgün, C. Z.; Makowski, L.; Atsumi, G.; Vaillancourt, E.; Kono, K.; Babaev, V. R.; Fazio, S.; Linton, M. F.; Sulsky, R.; Robl, J. A.; Parker, R. A.; Hotamisligil, G. S. *Nature* **2007**, *447*, 959.
- For a review see: Kralisch, S.; Fasshauer, M. *Diabetologia* **2013**, *56*, 10.
- Elmasri, H.; Ghelfi, E.; Yu, C.; Traphagen, S.; Cernadas, M.; Cao, H.; Shi, G.; Plutzky, J.; Sahin, M.; Hotamisligil, G.; Cataltepe, S. *Angiogenesis* **2012**, *15*, 457.
- Nieman, K. M.; Kenny, H. A.; Penicka, C. V.; Ladanyi, A.; Buell-Gutbrod, R.; Zillhardt, M. R.; Romero, I. L.; Carey, M. S.; Mills, G. B.; Hotamisligil, G. S.; Yamada, D. S.; Peter, M. E.; Gwin, K.; Lengyel, E. *Nat. Med.* **2011**, *17*, 1498.
- Levi, L.; Lobo, G.; Doud, M. K.; von Lintig, J.; Seachrist, D.; Tochtrop, G. P.; Noy, N. *Cancer Res.* **2013**, *73*, 4770.
- Sulsky, R.; Magnin, D. R.; Huang, Y.; Simpkins, L.; Taunk, P.; Patel, M.; Zhu, Y.; Stouch, T. R.; Bassolino-Klimas, D.; Parker, R.; Harrity, T.; Stoffel, R.; Taylor, D. S.; Lavoie, T. B.; Kish, K.; Jacobson, B. L.; Sheriff, S.; Adam, L. P.; Ewing, W. R.; Robl, J. A. *Bioorg. Med. Chem. Lett.* **2007**, *17*, 3511.
- Lan, H.; Cheng, C. C.; Kowalski, T. J.; Pang, L.; Shan, L.; Chuang, C.; Jackson, J.; Rojas-Triana, A.; Bober, L.; Liu, L.; Voigt, J.; Orth, P.; Yang, X.; Shipps, G. W., Jr.; Hedrick, J. A. *J. Lipid Res.* **2011**, *52*, 646.
- Lee, M. Y. K.; Li, H.; Xiao, Y.; Zhou, Z.; Xu, A.; Vanhoutte, P. M. *Br. J. Pharmacol.* **2011**, *162*, 1564.
- Barf, T.; Lehmann, F.; Hammer, K.; Haile, S.; Axen, E.; Medina, C.; Uppenberg, J.; Svensson, S.; Rondahl, L.; Lundbäck, T. *Bioorg. Med. Chem. Lett.* **2009**, *19*, 1745.
- Hertz, A. V.; Hellberg, K.; Reynolds, J. M.; Kruse, A. C.; Juhlmann, B. E.; Smith, A. J.; Sanders, M. A.; Ohlendorf, D. H.; Suttles, J.; Bernlohr, D. A. *J. Med. Chem.* **2009**, *52*, 6024.
- Ringom, R.; Axen, E.; Uppenberg, J.; Lundbäck, T.; Rondahl, L.; Barf, T. *Bioorg. Med. Chem. Lett.* **2004**, *14*, 4449.
- Ceccarelli, S. M.; Conte, A.; Kuehne, H.; Kuhn, B.; Neidhart, W.; Obst Sander, U.; Rudolph, M. WO 2,013,064,465; *Chem. Abstr.* **2013**, *158*, 679208.
- Hassan, M.; Brown, R. D.; Varma-O'Brien, S.; Rogers, D. *Mol. Divers.* **2006**, *10*, 283.
- Stahl, M.; Mauser, H.; Tsui, M.; Taylor, N. R. *J. Med. Chem.* **2005**, *48*, 4358.
- Hawkins, P. C. D.; Skillman, A. G.; Nicholls, A. *J. Med. Chem.* **2007**, *50*, 74.
- Aqueous solubility was measured by lyophilization solubility assay (LYSA). Solubility was measured from lyophilized DMSO stock solutions spectrophotometrically at pH 6.5 in a 50 mM phosphate buffer.
- Parallel artificial membrane permeation assay (PAMPA). See: Kansy, M.; Senner, F.; Gubernator, K. *J. Med. Chem.* **1998**, *41*, 1007.
- Kuhn, B.; Fuchs, J. E.; Reutlinger, M.; Stahl, M.; Taylor, N. R. *J. Chem. Inf. Model.* **2011**, *51*, 3180.